AIAA SciTech
13-17 January 2014, National Harbor, Maryland
52nd Aerospace Sciences Meeting

Flexible Thermal Protection System Physics-Based Modeling for Temperature Profile Predictions

Grant A. Rossman[1], John A. Dec[2], and Robert D. Braun[3]
Georgia Institute of Technology, Atlanta, GA, 30332

Candidate material testing was performed on various Flexible Thermal Protection Systems (FTPS) layup configurations in an arc-jet ground test facility. A physics-based thermal model was created to predict the thermal-material response of each FTPS layup under arc-jet induced thermal loading. Initial thermal model temperature predictions of embedded thermocouples for FTPS test articles showed an unsatisfactory correlation to arc-jet test data. The Levenberg-Marquardt (LM) inverse parameter estimation technique was implemented to reduce discrepancies between thermal model temperature predictions and experimental thermocouple temperature measurements by iteratively modifying FTPS thermal parameters within the model, such as thermal conductivity and specific heat. A formal parameter estimation methodology, previously applied for ablative TPS, is applied to this FTPS problem to improve understanding estimation behavior and LM error-minimization. Nominal, uncertainty, sensitivity, and inverse analysis are performed on scaled thermal inputs to provide insight on solution uniqueness and stability. This error-minimization technique is demonstrated on a previously flown FTPS layup configuration consisting of two outer fabric layers, two insulation layers, and one gas barrier layer. Results show that the LM method is a viable technique for inverse parameter estimation of FTPS thermal modeling problems.

Nomenclature

A	=	Entry vehicle drag area
C_D	=	Drag coefficient
C_P	=	Specific heat
k	=	Thermal conductivity
m	=	Entry vehicle mass
β	=	Ballistic coefficient
ε	=	Emissivity
ρ	=	Density
$f_{\varepsilon_{OF}}$	=	Scale factor for outer fabric emissivity
$f_{k_{OF}}$	=	Scale factor for outer fabric thermal conductivity
$f_{C_{p_{OF}}}$	=	Scale factor for outer fabric specific heat
$f_{k_{INS}}$	=	Scale factor for insulator thermal conductivity
$f_{C_{p_{INS}}}$	=	Scale factor for insulator specific heat
$f_{\rho_{INS}}$	=	Scale factor for insulator density
$f_{C_{p_{GB}}}$	=	Scale factor for gas barrier specific heat
P	=	Scale factor thermal input parameter vector
T	=	Temperature profile prediction vector from COMSOL
Y	=	Thermocouple measured experimental temperature vector

[1] Graduate Research Assistant, Guggenheim School of Aerospace Engineering, AIAA Student Member.
[2] Aerospace Engineer, NASA Langley Research Center, AIAA Student Member.
[3] David and Andrew Lewis Professor of Space Technology, Guggenheim School of Aerospace Engineering, AIAA Fellow.

$\mathbf{J}$ = Sensitivity matrix
μ = Damping parameter
Ω = Diagonal matrix
k = Error-minimization iteration number
S = Error-minimization objective function
ε_0 = Central difference method tolerance
ε_1 = Stopping criteria 1 tolerance
ε_2 = Stopping criteria 2 tolerance
ε_3 = Stopping criteria 3 tolerance

I. Introduction

ENTRY, Descent, and Landing (EDL) describes the process of safely bringing a spacecraft to rest on the surface of an atmospheric body. For Mars EDL, the Viking entry vehicle design has been incrementally improved during the past two decades to increase landing mass capability. Previous missions laid the ground work for current State of the Art (SOA) rigid aeroshells. Additionally, rigid ablators like the Super Lightweight Ablator (SLA-561V) and Phenolic Impregnated Carbon Ablator (PICA) have been used on every Mars mission to date.[1] Landing additional mass beyond the Mars Science Laboratory (MSL) capability has been shown to be difficult with present technology, motivating the advancement of technologies to enable future missions. One such technology is a hypersonic inflatable aerodynamic decelerator (HIAD).

A HIAD is an inflatable device that produces a large drag area, and as a result, reduces the entry ballistic coefficient shown in Equation 1 below.

$$\beta = \frac{m}{C_D A} \tag{1}$$

Ballistic coefficient is a function of the vehicle mass, drag coefficient, and reference area. HIADs reduce the vehicle's ballistic coefficient with a substantial increase in drag area while adding minimal mass. A lower ballistic coefficient allows the vehicle to decelerate higher in the atmosphere, decreasing the peak heat rate experienced by the HIAD TPS.[2]

Unlike rigid TPS, HIAD TPS must remain flexible to allow for packaging within the confines of a launch vehicle shroud prior to withstanding aerothermal loading. The FTPS must not experience performance degradation from multiple packing and unpacking cycles.[3] With the advancement of fabric and thin-film materials, FTPS material development for HIADs may result in a means to increase mission capabilities. By making improvements in thermal modeling, designers can obtain more accurate and more reliable FTPS mass estimations for future Earth and Mars entry missions.

NASA has increased the flight readiness of FTPS materials through several development efforts.[4] The research presented here extends the HIAD FTPS predictive capability by developing a detailed physics based model, using a multi-parameter error-minimization technique to attempt validation with ground-based test data. The long-term goal of this research is to develop a robust error-minimization methodology that can be applied across a wide range of candidate FTPS materials while allowing for addition or removal of physical processes as needed. The resulting error-minimization technique will be extended to similar layups and exposed to various arc-jet heat fluxes and pressure combinations in an effort to extend thermal model development, as described in the future work section.

The thermal model is being developed using COMOSL Multi-Physics software. Creating a thermal model that accurately predicts temperatures within an FTPS layup requires detailed understanding of the physical processes and thermal properties associated with each material layer. The thermal properties associated with the candidate FTPS materials are also functions of temperature and pressure, adding to the non-linear behavior of thermal response. The first stage in developing a thermal model is to ensure all the pertinent physical processes are included and all thermal properties have been verified through property testing over the appropriate temperature and pressure range of interest. Next, the model must be validated by comparing arc-jet test temperature data to the one-dimensional (1D) thermal response of the FTPS COMSOL model. Finally, the performance of the COMSOL model is evaluated based on how closely the 1D model temperature predictions match the arc-jet thermocouple temperature data for each thermocouple.

As is often the case, the mathematical model's temperature predictions do not exactly match arc-jet experimental data for various reasons. Some examples include, but are not limited to, uncertainty in the material properties used in

the mathematical model, uncertainty in the arc-jet tunnel conditions, and small errors in the thermocouple measurements themselves. To improve model correlation to the test data, small corrections to the thermal input parameters are required. It should be noted that manipulating the thermal parameters to achieve correlation incorporates all the other uncertainties in the system and transfers them to the thermal parameters. It is common practice for analysts working with rigid, ablative TPS to achieve data correlation by only adjusting the material's char thermal conductivity. These corrections are typically made using a time-consuming, manually iterative approach in which char conductivity is adjusted. The resulting predictions are compared to measured data and this process is iteratively repeated until a satisfactory correlation is achieved. While this model tuning process has been shown to produce reasonable results, it is disadvantaged by representing model uncertainty with a single parameter. Additionally, tuning adjustments made by different analysts are likely to produce different models of the same system. The objective of this research is to develop an inverse analysis methodology to correlate FTPS thermal model temperature predictions to measured temperatures from arc-jet experimental data. This technique will manipulate multiple thermal model input parameters simultaneously using established inverse estimation theory.

II. FTPS Experimental Testing and Evaluation

The purpose of FTPS is to protect the HIAD inflatable drag device from the harsh aerothermodynamic environment of atmospheric re-entry. The composite FTPS material layup must withstand the heat loads and aerodynamic forces, which create many design requirements. There are two main areas of exploration with regards to FTPS, which include gathering composite thermo-mechanical properties of each layup and accurately modeling the thermal response with computer software. Both areas are enabled by experimental testing at relevant mission conditions. A wide range of testing facilities were considered for overall FTPS material characterization.[3,5] Although it would be ideal to test under exact flight conditions, there are no ground-based facilities that can simultaneously match all of the flight conditions in terms of heat flux, surface pressure, and enthalpy. The most capable facility for re-creating expected aerothermodynamic conditions for the Inflatable Re-entry Vehicle Experiment-3 (IRVE-3) and the High Energy Atmospheric Re-entry Test (HEART) is the Boeing Large Core Arc Tunnel (LCAT) Facility.[5] Significant focus has been placed on developing the specific methodology for modeling and simulation of FTPS test runs in the Boeing LCAT facility located in St. Louis, Missouri.[5] The long-term goal of this research is to acquire the ability to predict measured thermocouple temperatures from various LCAT runs within the specified heat flux and pressure ranges.

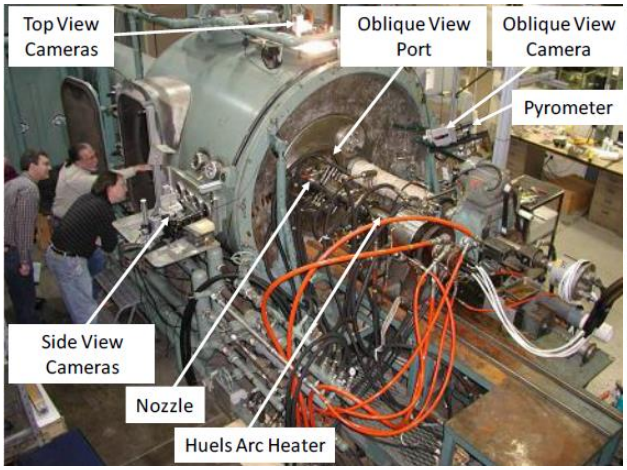

Figure 1. Boeing Large Core Arc Tunnel (LCAT)[5]

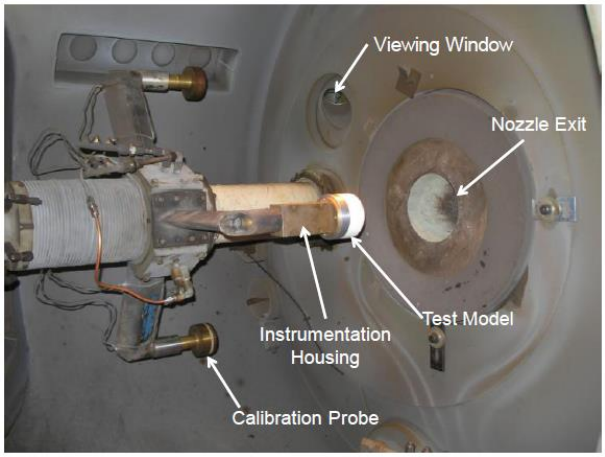

Figure 2. Boeing LCAT Stagnation Test Sting Arm[5]

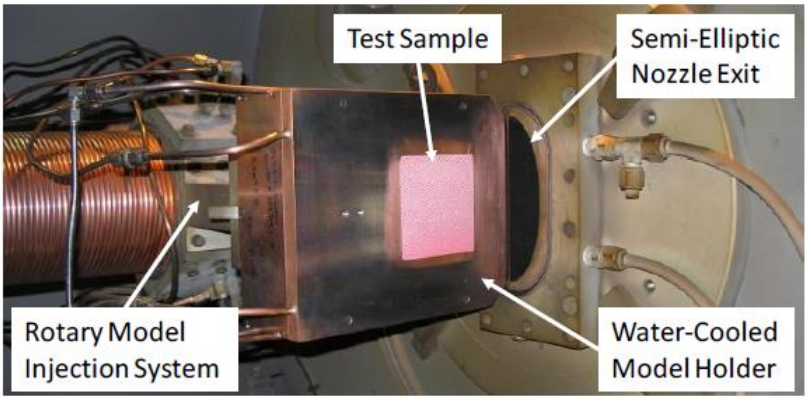

Figure 3. Boeing LCAT Shear Test Configuration[5]

The Boeing LCAT facility makes uses of a Huels arc-heater to raise the temperature of supersonic flow through the pressurized test cabin.[5] An external photograph of the test cabin is provided in Figure 1 above. Flow coming out of the exit nozzles shown in Figure 2 and Figure 3 hit the FTPS sample held by the proper shear or stagnation test fixtures. For shear tests, a custom-developed wedge model was loaded with the FTPS sample and adjusted to the correct angle to achieve the target shear force, surface pressure, and heat flux for each free-jet shear test.[5] The shear test fixture used for Run 2259 is shown above in Figure 3 using a semi-elliptic nozzle exit to properly displace the flow over the sample. The water-cooled, copper model holder used to perform stagnation testing on Run 2330 is shown above in Figure 2.[5] Table 1 below shows the Boeing LCAT testing conditions for Layup 1's Run 2259 (shear test) and Layup 2's Run 2330 (stagnation test).

Table 1. Boeing LCAT Testing Conditions for Run 2259 and Run 2330[6]

LCAT Run Number	Layup Configuration	Probe Heat Flux (W/cm^2)	Surface Pressure (kPa)
2259	Layup 1	26.7	8.01
2330	Layup 2	21.4	3.1

In general, FTPS consists of multiple layers, each with a unique function. The first set of layers, referred to as the outer fabric, is a porous fabric meant to protect the underlying layers from the incident heat flux. The second set of layers, referred to as the insulator, is a porous insulation sheet that further prevents through-thickness heat conduction, keeping the interface to the inflatable structure. The last layer, referred to as the gas barrier, is a sheet of Aluminized Kapton laminated to Kevlar that prevents flow from traveling through the entire layup. The gas barrier also behaves as the interface between the FTPS and the vehicle's inflatable structure, which is equivalent to the "bondline" for an ablative heat shield system.

Between 2011 and the present, there have been various arc-jet tests performed to help qualify the FTPS material for upcoming flight missions mentioned above. Both stagnation and shear tests have been performed on various FTPS layup material combinations in order to find an optimum configuration. Layup combinations have considered two outer fabrics (Nextel BF-20 and Silicon Carbide), six insulators (Pyrogel 3350, Pyrogel 2250, Saffil, Polyimide, APA, and APA2), and two gas barriers (Aluminized Kapton Kevlar and Kapton Kevlar Laminate). Although LCAT arc-jet testing initially operated using a square heat flux profile for FTPS layups, recent arc tunnel upgrades now allow layups to be tested using more flight-like heat-flux profiles where the heat flux changes over time.

Because the set of outer fabric and insulation layers are porous and allow gas to flow through, it was critically important to match surface pressure to the desired flight condition during testing to obtain an accurate thermal response for each layup. Each layup configuration was subjected to LCAT stagnation testing to characterize thermal performance and shear testing to analyze mechanical properties. Thermocouples placed between FTPS layers at various depths measure temperature vs. time during experimental testing. A pyrometer is used to estimate the outer fabric top surface temperature. Although both stagnation and shear testing are both important for creating a final FTPS design, this analysis will focus on specific LCAT stagnation tests for development of the proposed multi-parameter error-minimization using the LM method.

III. FTPS Thermal Model Development

While many different layup configurations have been tested in the Boeing LCAT facility, two similar configurations will be investigated in this analysis, referred to as Layup 1 (L1) and Layup 2 (L2). Both layups contain Nextel BF-20 as the outer fabric, Aspen Aerogel's Pyrogel 3350 (Layup 1) or Pyrogel 2250 (Layup 2) as the insulator, and Aluminized Kapton laminated to Kevlar as the gas barrier. Additionally, a thermocouple (TC) temperature measurement device is placed between each FTPS layer to obtain experimental temperature measurements at multiple depths. Graphics describing the material and thermocouple configurations for Layup 1 and Layup 2 are shown below in Figure 4 and Figure 5, respectively. The set of outer fabric layers for both layups is composed of Nextel BF-20 ceramic fabric. However, the set of insulator layers are independent, as Layup 1 uses Aspen Aerogel's Pyrogel 3350 and Layup 2 uses Aspen Aerogel's Pyrogel 2250.

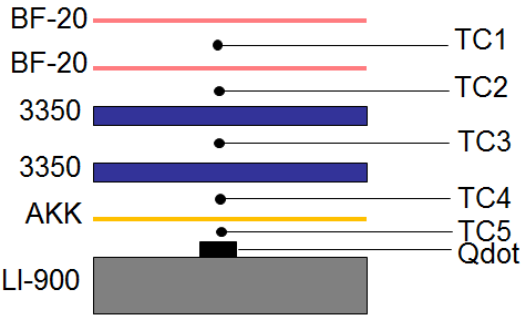

Figure 4. L1 (LCAT 2259-BF-20, Pyrogel 3350, AKK)[7]

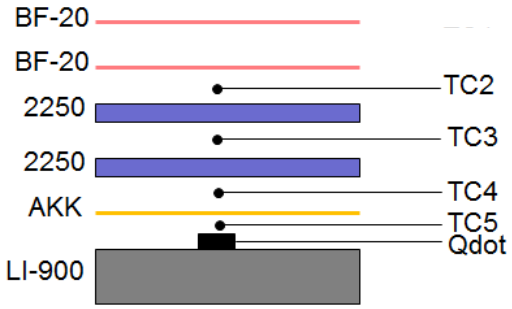

Figure 5. L2 (LCAT 2330 - BF-20, Pyrogel 2250, AKK)[7]

Using the COMSOL Mutli-Physics software framework, the many physical processes experienced during arc-jet testing have been combined within one cohesive thermal model, which includes the governing equations for conservation of mass, momentum, and energy. Southwest Research Institute (SRI) successfully performed various experiments on FTPS material samples to obtain measured values of the thermophysical properties. The material property databases for virgin and charred FTPS layers are input into the model in tabular form. Additionally, these properties are input as a function of temperature and pressure. Performing FTPS testing in the Boeing LCAT facility helps analysts gain a deeper understanding of the complex thermal response of these materials and obtain thermocouple measurements from which the mathematical model can be compared.

Thermal conductivity for the insulator materials is made up of the sum of three components: solid conduction, gas conduction, and internal radiation. After performing experimental testing, it was shown that as Pyrogel 3350 is heated to the region between 375˚C and 600˚C, it begins to shrink in size while decomposing and emitting gases as a result of pyrolysis. The decomposition and pyrolysis gas flow are energy absorbing mechanisms that potentially lower the temperatures through a FTPS layup.[4] Pyrogel 2250 exhibits similar decomposition and pyrolysis behavior, which must be accounted for in the thermal model before accurate temperature predictions can be made. Complex phenomena such as the potential for boundary layer flow through the porous outer fabric and insulation layers and pyrolysis gas flow to the surface through these layers will also be added to the model for higher fidelity. Understanding the decomposition of both Pyrogel 3350 and Pyrogel 2250 as a function of temperature, pressure, and time is crucial to obtaining successful temperature predictions. The thermal model has successfully modeled convection, surface radiation, and solid/gas conduction through FTPS layers. The current model includes the capability to incorporate insulator pyrolysis gas flow and decomposition but remains unused until the permeability is characterized for each FTPS layer.[3] Additionally, the pyrolysis gas species generated from decomposition are still being characterized and will also be added to the model.

Preliminary results indicate that the thermal model consistently over-predicts thermocouple temperatures when compared with measured arc-jet data, as will be discussed in great detail in following sections. Temperature predictions for the bondline interface, which sits between the bottom insulator layer and the gas barrier, consistently over-predicts temperature measurements. While this conservative estimate leads to a "safer" FTPS design, these predictions could produce an FTPS mass beyond requirements, which adds unnecessary to mass and ultimately decreases usable payload mass. Once the thermal model can be validated with accurate thermocouple temperature predictions, the model can be integrated into a probabilistic heat shield sizing process to avoid unnecessarily "over-margining" heat shield thickness. In order to minimize the thermal model's temperature prediction gap and progress towards model validation, a parameter estimation technique called the Levenberg-Marquardt (LM) method will be

applied directly to the COMSOL thermal model to estimate FTPS thermophysical properties that reduce prediction discrepancies.

IV. Parameter Estimation Methodology Using the Levenberg-Marquardt Technique

While there are many thermal properties to consider when making temperature predictions, this initial thermal model focuses on accurate estimation of emissivity, specific heat, and thermal conductivity for each layer of material. As there are 3 sets of material layers in both Layup 1 and Layup 2, 9 thermal parameters were initially considered as design variables for error-minimization for each layup. After performing an effects screening sensitivity analysis to find out which parameters contribute most to the variability of thermal response, 2 of these 9 initial parameters could be eliminated, leaving 7 thermal parameters for estimation. The final design variables are the outer fabric (OF) emissivity ($f_{\varepsilon_{OF}}$), OF thermal conductivity ($f_{k_{OF}}$), OF specific heat ($f_{C_{p_{OF}}}$), insulator (INS) thermal conductivity ($f_{k_{INS}}$), INS specific heat ($f_{C_{p_{INS}}}$), INS density ($f_{C_{p_{INS}}}$), and gas barrier (GB) specific heat ($f_{C_{p_{GB}}}$). These design variables used in error-minimization are not the thermal parameters themselves, but corresponding scale factors. This approach enables quick determination of the percent change of each thermal parameter and avoids discontinuous behavior. The following scale factor parameter vector **P** for error-minimization iteration step "k" is shown by Equation 2 below:

$$\mathbf{P}^{k} = \left[f_{\varepsilon_{OF}}, f_{k_{OF}}, f_{C_{p_{OF}}}, f_{k_{INS}}, f_{C_{p_{INS}}}, f_{\rho_{INS}}, f_{C_{p_{GB}}}\right] \tag{2}$$

The Levenberg-Marquardt (LM) method is frequently used for ill-conditioned inverse heat transfer problems. Using an iterative process and a sensitivity matrix composed of first-order partial derivatives of scaled thermal input parameters at each time step, the user solves a least squares minimization problem to obtain a minimized solution.[8] The LM technique behaves like a steepest descent algorithm near the starting point, and as the solution approaches a minimum, it exhibits similar behavior to Gauss' method.[8,9,10] The following discussion provides a step-by-step walkthrough of the calculations performed by the LM method to minimize error between thermocouple predictions and arc-jet thermocouple measurements.

Step 1: Solve the direct heating problem with $\mathbf{P}^{k}$ (current step parameter estimates) to obtain $T(\mathbf{P}^{k})$ (predicted temperatures)

Step 2: Compute the objective function $S(\mathbf{P}^{k})$ using the equations defined below.

$$S(\mathbf{P}^{k}) = [\mathbf{Y} - \mathbf{T}(\mathbf{P}^{k})]^{T}[\mathbf{Y} - \mathbf{T}(\mathbf{P}^{k})] \tag{3}$$

$$S(\mathbf{P}^{k}) = \sum_{i=1}^{I}(Y_i - T_i(\mathbf{P}^{k}))^2 \tag{4}$$

Step 3: Compute the sensitivity matrix $\mathbf{J}^{k}$ using the following equation.

$$\mathbf{J}(\mathbf{P}) = \left[\frac{\partial \mathbf{T}^{T}(\mathbf{P})}{\partial \mathbf{P}}\right]^{T} = \begin{bmatrix} \frac{\partial T_1}{\partial P_1} & \frac{\partial T_1}{\partial P_2} & \frac{\partial T_1}{\partial P_3} & \cdots & \frac{\partial T_1}{\partial P_N} \\ \frac{\partial T_2}{\partial P_I} & \frac{\partial T_2}{\partial P_2} & \frac{\partial T_2}{\partial P_3} & \cdots & \frac{\partial T_2}{\partial P_N} \\ \vdots & \vdots & \vdots & & \vdots \\ \frac{\partial T_I}{\partial P_I} & \frac{\partial T_I}{\partial P_2} & \frac{\partial T_I}{\partial P_3} & \cdots & \frac{\partial T_I}{\partial P_N} \end{bmatrix} \tag{5}$$

The central difference approximations is used to calculate each sensitivity coefficient, where $\varepsilon_0 \approx 10^{-5}$ as shown below.

$$J_{ij} \cong \frac{\partial T_i}{\partial P_j} = \frac{T_i(P_1, P_2, \ldots, P_j + \varepsilon P_j, \ldots, P_N) - T_i(P_1, P_2, \ldots, P_j - \varepsilon P_j, \ldots, P_N)}{2\varepsilon_0 P_j} \tag{6}$$

Using an initial scale factor vector, $\mathbf{P}^{\mathrm{k}}$, the LM method uses a sensitivity matrix $\mathbf{J}^{k}$ to determine the proper $\Delta\mathbf{P}^{k}$ to apply at each iteration, "k", in order to approach the minimized scale factor combination, $\mathbf{P}^{\mathrm{k+1}}$

Step 4: Solve the following linear system of equations to find $\Delta\mathbf{P}^{k}$(suggested change in current parameter vector estimate)

$$\Omega^{\mathrm{k}} = \mathrm{diag}\left[(\mathbf{J}^{\mathrm{k}})^{\mathrm{T}}\mathbf{J}^{\mathrm{k}}\right] \tag{7}$$

$$\left[(\mathbf{J}^{\mathrm{k}})^{\mathrm{T}}\mathbf{J}^{\mathrm{k}} + \mu^{\mathrm{k}}\Omega^{\mathrm{k}}\right]\Delta\mathbf{P}^{\mathrm{k}} = (\mathbf{J}^{\mathrm{k}})^{\mathrm{T}}\left[\mathbf{Y} - \mathbf{T}(\mathbf{P}^{\mathrm{k}})\right] \tag{8}$$

$$\Delta\mathbf{P}^{k} = \left[(\mathbf{J}^{\mathrm{k}})^{\mathrm{T}}\mathbf{J}^{\mathrm{k}} + \mu^{\mathrm{k}}\Omega^{\mathrm{k}}\right]^{-1}(\mathbf{J}^{\mathrm{k}})^{\mathrm{T}}\left[\mathbf{Y} - \mathbf{T}(\mathbf{P}^{\mathrm{k}})\right] \tag{9}$$

Step 5: Compute the new estimate $\mathbf{P}^{\mathrm{k+1}}$ using the following equation

$$\mathbf{P}^{\mathrm{k+1}} = \mathbf{P}^{\mathrm{k}} + \Delta\mathbf{P}^{k} \tag{10}$$

Step 6: Solve the direct problem with the new estimate of parameters $\mathbf{P}^{\mathrm{k+1}}$ to obtain the predicted temperatures $\mathbf{T}(\mathbf{P}^{\mathrm{k+1}})$. Compute the new objective function $S(\mathbf{P}^{k+1})$.

Step 7: If $S(\mathbf{P}^{k+1}) \geq S(\mathbf{P}^{k})$, replace μ^{k} by $10\mu^{\mathrm{k}}$ and return to step 4.

Step 8: If $S(\mathbf{P}^{k+1}) < S(\mathbf{P}^{k})$, accept the new estimate $\mathbf{P}^{\mathrm{k+1}}$ and replace μ^{k} by $0.1\mu^{\mathrm{k}}$.

Both Step 7 and Step 8 were modified as necessary in order to more finely tune the performance of the error-minimization code. Resetting values for μ^{k} in Steps 7-8 and ε_0 in Equation 6 is discussed in detail with the TC3 driver approach code verification portion of the Results section. Note that the TC3, or in general, TCX nomenclature refers to the thermocouple placement shown in Figure 4 and Figure 5.

Step 9: As a last step, one must implement stopping criteria. If the stopping criterion is satisfied, stop the iterative procedure; otherwise replace *k* by *k+1* and return to step 3. The following equations are examples of stopping criteria:

$$\left|S(\mathbf{P}^{k+1}) - S(\mathbf{P}^{k})\right| < \varepsilon_1 \tag{11}$$

$$\left\|\mathbf{P}^{\mathrm{k+1}} - \mathbf{P}^{\mathrm{k}}\right\| < \varepsilon_3 \tag{12}$$

In this initial setup of the LM error-minimization architecture, TC4 of the FTPS layup will be considered the "bondline" thermocouple and will be the only sensor used for analysis. To begin the error-minimizing process, one starts with the first step of using the initial scale factors, $\mathbf{P}^{\mathrm{k}}$, and uses the COMSOL thermal model of Layup 1 to calculate the corresponding predicted temperature profiles for each thermocouple of interest. In this case, the analyst is interested in only TC4 temperature profile predictions. The following discussion describes the results generated from applying the LM Method for FTPS error-minimization of Layup 1 above. [8]

V. Results

Arc-jet testing was conducted on FTPS material layups in order to characterize thermal material performance with the goal of choosing a next-generation FTPS layup to be used on future HIAD missions. Thermocouples were placed between each FTPS layer during testing to obtain temperature vs. time profile measurements at various depths (TC1, TC2, TC3, and TC4 from Figure 4). A physics-based model was created in COMSOL to generate corresponding thermocouple temperature vs. time profile predictions at the same arc-jet testing depths (TC1, TC2, TC3, and TC4 from Figure 4). The goal of the modeling effort is to produce thermocouple predictions within an acceptable closeness to thermocouple measurements. The thermal model initially solves the direct heat transfer problem by accepting arc-jet measured heat flux as the driving boundary condition on the top surface of Layup 1 and solving for temperature predictions at the appropriate depths. Discrepancies produced by the model itself and by uncertain knowledge of the boundary condition are expected to cause initial predictions to deviate from measurements. Parameter estimation is commonly used to reduce prediction errors by accurately estimating

thermophysical parameters within the model.[12] Thermophysical properties can be measured with confidence, albeit with some uncertainty, using traditional methods. Generally, material property testing is limited in range in both temperature and pressure and is also obtained at discrete points. Moreover, the arc-jet test conditions have the potential of producing temperatures that exceed that of which the data was collected. In these cases, the data in the thermal model is extrapolated to provide a contiguous set of data. The capability does exist to make property measurements in high temperature regions around 2000°C. In general, the uncertainty in the measurement grows as temperature increases. Therefore, the primary motivation to perform parameter estimation is to minimize COMSOL thermal model temperature prediction discrepancies by more accurately estimating these FTPS thermophysical properties during extreme regions of arc-jet testing where materials experience temperatures and pressures outside their known and tested limits, or in regions where the uncertainty in the measured properties is large.

The LM method discussed in the previous section has been selected as a candidate for thermophysical parameter estimation to reduce model discrepancy. The following discussion provides results for a successfully completed parameter estimation using the LM Method. The COMSOL model will be used to produce initial thermocouple temperature predictions of Layup 1 from Run 2259. The LM method will be implemented to estimate thermophysical properties of interest to show initial LM error-minimization. After performing a literature search, a parameter estimation methodology will be implemented to gain a deeper understanding of the problem by addressing solution uniqueness and stability directly. The boundary condition applied to the model will be changed from a heat-flux applied to the surface of the FTPS layup (heat flux driver approach) to applying measured TC3 data at the appropriate depth to solve for TC4 predictions (TC driver approach). Finally, a test problem will be solved using the LM method with the TC driver approach to minimize error between Layup 1-TC4 predictions and arc-jet measurements from Run 2259.

Initial thermal model predictions are provided below for Boeing LCAT Run 2259 (shear-test for Layup 1) and Run 2330 (stagnation-test for Layup 2) in Figure 6 and Figure 7, respectively. The "TCX – Data" curves represent arc-jet measured thermocouple temperatures while the "TCX – Nom" curves display initial thermal model predictions.

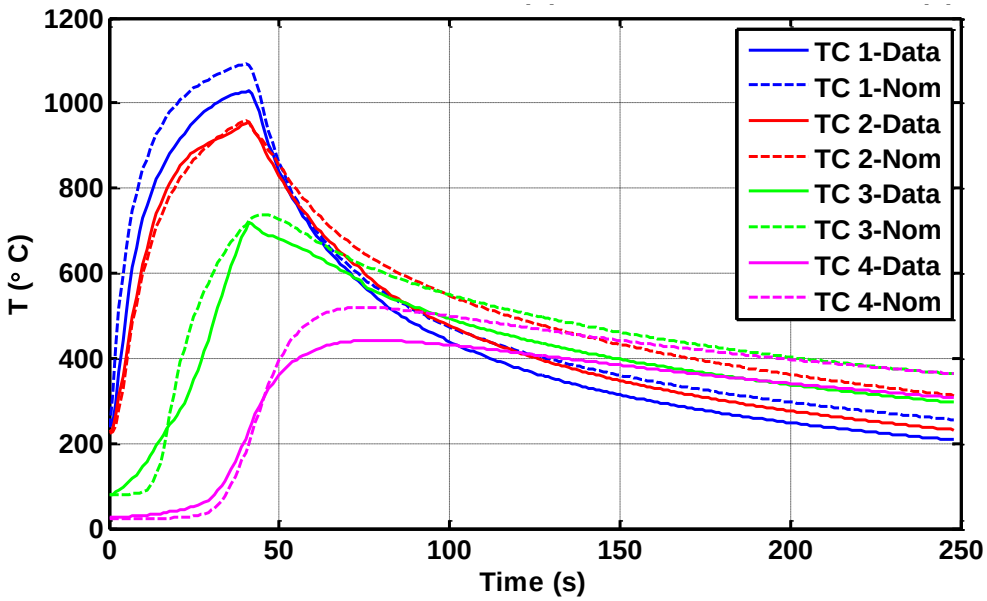

Figure 6. Initial COMSOL Thermal Model Prediction of TC-4 for Run 2259

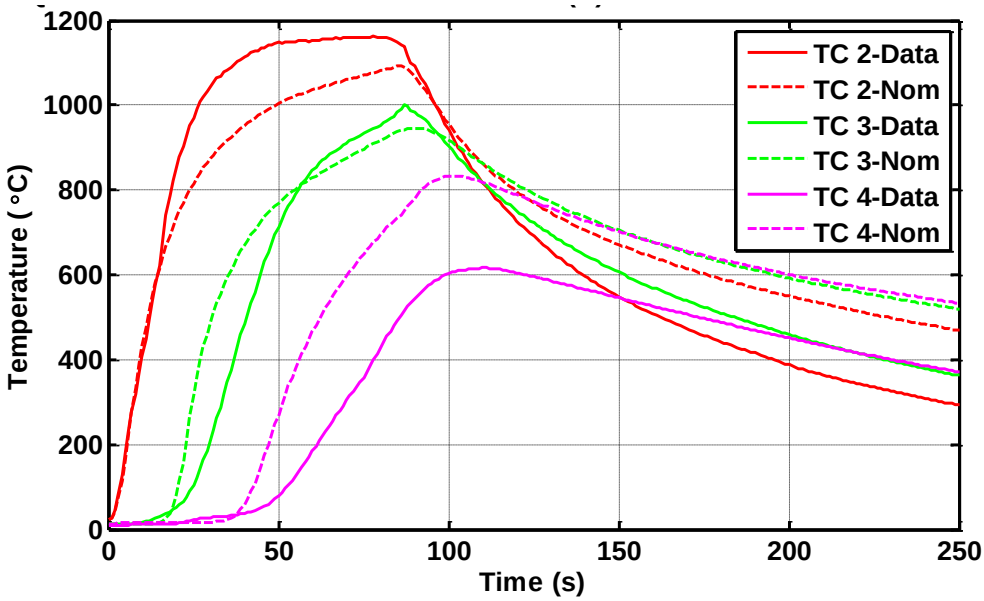

Figure 7. Initial COMSOL Thermal Model Prediction of TC-4 for Run 2330

As illustrated, the predictions for bondline TC4 are much more accurate in Run 2259 than in Run 2330, but neither matches the data exactly. Before performing parameter estimation, it is crucial to select an acceptable arc-jet data set for comparison. In general, parameter estimation is much more effective when initial predictions are close because there is less model error for the thermophysical parameters to overcome. Both Run 2259 and Run 2330 exhibit equivalent prediction proximity for TC2 and TC3. Since the objective function of the LM method only considers prediction discrepancies for TC4, Run 2259 was chosen for further analysis.

A. Initial Levenberg-Marquardt Parameter Estimation using Heat Flux Driver COMSOL Model

Now that Run 2259 has been selected for further analysis, we must select the FTPS parameters we wish to estimate. The thermophysical properties accounted for in the COMSOL model for each layer include thermal conductivity (κ), specific heat (Cp), density (ρ), emissivity for outer-fabric layers (ε), and thickness for insulation layers (t). Considering four different thermophysical properties for three different material types, a preliminary sensitivity analysis was performed on the model to determine which of these twelve thermophysical parameters is statistically significant. The seven parameters that exhibited statistical significance include the parameters mentioned previously ($f_{\varepsilon_{OF}}$, $f_{k_{OF}}$, $f_{C_{p_{OF}}}$, $f_{k_{INS}}$, $f_{C_{p_{INS}}}$, $f_{\rho_{INS}}$, $f_{C_{p_{GB}}}$). In order to set constraints for the LM error-minimization, each scale factor was given upper and lower bounds, which are treated as classical optimization side constraints. The small and large side-constraint ranges are listed in Table 2 below:

Table 2. Small and Large Range Side Constraint Upper and Lower Bounds for Scale Factors

Side Constraint Bounds	$f_{\varepsilon_{OF}}$	$f_{k_{OF}}$	$f_{C_{p_{OF}}}$	$f_{k_{INS}}$	$f_{C_{p_{INS}}}$	$f_{\rho_{INS}}$	$f_{C_{p_{GB}}}$
Small-Range Upper Bound	1.05	1.25	1.10	1.25	1.10	1.10	1.10
Small-Range Lower Bound	0.95	0.75	0.90	0.75	0.90	0.90	0.90
Large-Range Upper Bound	1.15	1.50	1.30	1.50	1.30	1.30	1.30
Large-Range Lower Bound	0.85	0.50	0.70	0.50	0.70	0.70	0.70

The direct problem in heat transfer analysis solves for unknown temperatures at depth performing calculations with known boundary conditions and thermophysical properties. With regards to the COMSOL model, the thermocouple temperatures (TC1 – TC4) are solved for using a known heat flux as the surface boundary condition and estimated thermal properties of each FTPS layer. Thermophysical properties of FTPS layers may be measured within a specific environment using experimental techniques. Obtaining true properties because much more difficult

under extreme environmental conditions, such as high temperature and pressure applied to the FTPS stack. Inverse Parameter Estimation (IPE) methods allow estimation of these thermophysical properties.[11] Because it was shown that the initial COMSOL model predictions deviated significantly from test data in Figure 3, a parameter estimation must be performed to reconcile the differences.[8] Figure 8 below shows the results of an initial LM error-minimizing attempt considering only TC4 prediction errors in the LM method's objective function ($S(\mathbf{P}^k) = [\mathbf{Y} - \mathbf{T_{TC4}}(\mathbf{P}^k)]^T[\mathbf{Y} - \mathbf{T_{TC4}}(\mathbf{P}^k)]$). All seven scale factors of statistical significance mentioned above were varied within their small side-constraint range upper and lower bounds specified in Table 2 above to produce these results shown in Figure 8 below:

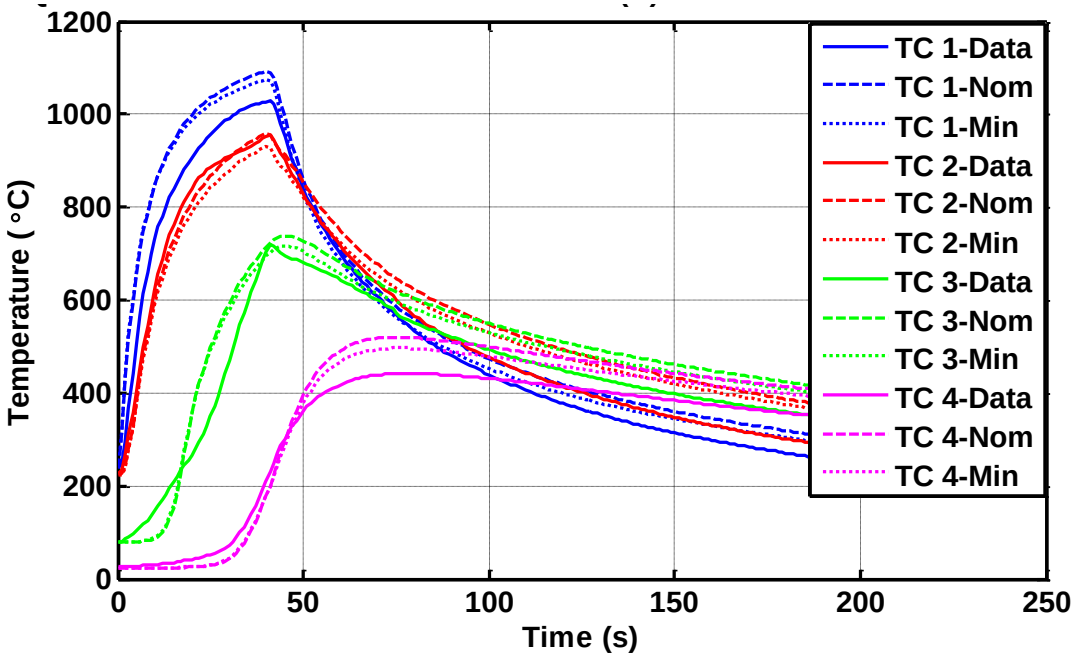

Figure 8. Error-Minimized TC-4 Bondline Predictions for Run 2259 Small Side-Constraint Range

The implemented LM parameter estimation in Figure 8 resulted in slightly improved TC4 model predictions shown by the "TC4-Min" prediction profile curve moving closer to the "TC4-Data" measured arc-jet prediction profile. Although improvement is achieved, it is not significant enough to deem acceptable. As the following discussion will point out, much more analysis is required to perform a more intelligent and effective LM error-minimization. Results will show that not all seven scale factors can be estimated simultaneously and the scale factor vector must be reduced to improve solution uniqueness and stability.

B. Application of Parameter Estimation Methodology to Heat Flux Driver COMSOL Model for Run 2259

After performing an initial error-minimization using the LM method mentioned above, a literature search was performed to delve more deeply into the topic of Inverse Parameter Estimation (IPE). The goal of this literature search was to gain a more fundamental understanding of the thermophysical parameters and provide supporting analyses beforehand to improve the performance of the LM error-minimization on the heat flux driver model. Molavi performs a detailed analysis applying the Levenberg-Marquardt technique to a thermophysical parameter estimation problem for rigid, noncharring ablators.[11] In addition to providing information regarding numerical computations of the LM method for inverse analysis, Molavi discusses sensitivity analysis of thermophysical parameters as a useful tool to determine each parameter's linear-dependence on the rest of the parameters. Two parameters that are linearly-dependent and strongly correlated have similar or exactly opposing effects on the temperature predictions of the model. Due to this dependency, the LM method cannot distinguish the individual effects of each correlated, linearly-dependent parameter during the error-minimization process, leading to challenges with solution uniqueness. Understanding relative parameter correlation provides valuable information about which thermophysical parameters can be estimated simultaneously to obtain a unique solution.

In a similar study, Mahzari develops an inverse parameter estimation methodology with the goal of estimating thermophysical properties for embedded thermocouples on the ablative heatshield of Mars Science Laboratory (MSL).[9] In addition to sensitivity analysis of parameters, Mahzari performs nominal and uncertainty analyses before inverse parameter estimation to consider high-quality measurement data and identify each parameter's percent contribution to temperature prediction uncertainty. To improve the LM method's ability to minimize model error, the described parameter estimation architecture was implemented. First, a nominal analysis was performed to investigate the state of the arc-jet test data and specify which portion of Run 2259 will be considered in the LM objective function. Next, a transient uncertainty analysis was performed for each thermocouple in Layup 1 to investigate the contribution of each scale factor to the thermal model's temperature prediction uncertainty. Finally, a sensitivity analysis was performed for Layup 1 to examine the correlations between scale factors and gain insight on solution uniqueness and stability. All analyses help better inform LM error-minimization by selecting the appropriate thermophysical properties to estimate within the thermal model.

Nominal analysis is performed using Figure 8 above. As mentioned, the initial COMSOL model predicts TC4 within a reasonable range for the first 40 seconds. The moment that the heat flux boundary condition is removed (to represent model retraction) TC4 predictions overshoot the measured bondline peak temperature and remain at a higher temperature throughout cool-down. Since the COMSOL model is one-dimensional in the through-thickness direction, it does not capture two-dimensional and three-dimensional heat transfer effects. Additionally, pyrolysis gas flow is not considered through FTPS layers in the model, which leads to thermocouple overprediction when pyrolysis occurs at peak bondline temperatures. Finally, the thermal model does not account for the water cooled model holders continuing to pull heat out of the FTPS stack up during the cool-down process, which lowers arc-jet measured thermocouple temperatures following model retraction. Therefore, for TC4 in Run 2259, predictions should only be considered when heat flux is the dominant method of heat transfer, or within the first portion of the run. The thermal model does not yet incorporate all physical phenomena occurring during cool-down and inclusion of these will be left for future work. With this information in mind, the objective function used by the LM method, $(S(\mathbf{P}^k) = [\mathbf{Y} - \mathbf{T_{TC4}}(\mathbf{P}^k)]^{\mathrm{T}}[\mathbf{Y} - \mathbf{T_{TC4}}(\mathbf{P}^k)])$, should only consider comparing predictions during FTPS heat up, starting with model injection at t = 0 seconds and ending with TC4 bondline peak temperature at approximately t = 80 seconds.

Uncertainty analysis is performed to determine which thermal scaling parameters contribute most to the uncertainty of predicted thermocouple temperature profiles generated by the COMSOL model. Uncertainty analysis was performed with a Monte Carlo simulation using five-thousand normally distributed values for input scaling parameter uncertainties within the small side-constraint range specified above. After feeding these randomly generated inputs into the COMSOL thermal model, five-thousand resulting temperature profiles were generated for each thermocouple (TC1-TC4). These temperature profiles are depicted in Figure 9 – Figure 12 below, showing the resulting temperature profile dispersion across the small side-constraint range of scale factor values.

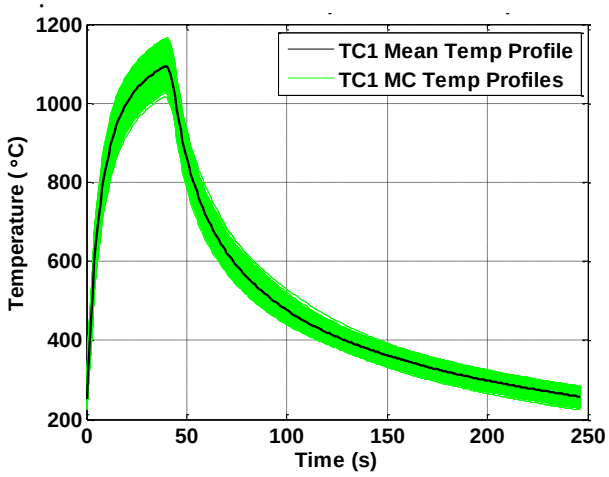

Figure 9. TC1 MC Temperature Profile Spread

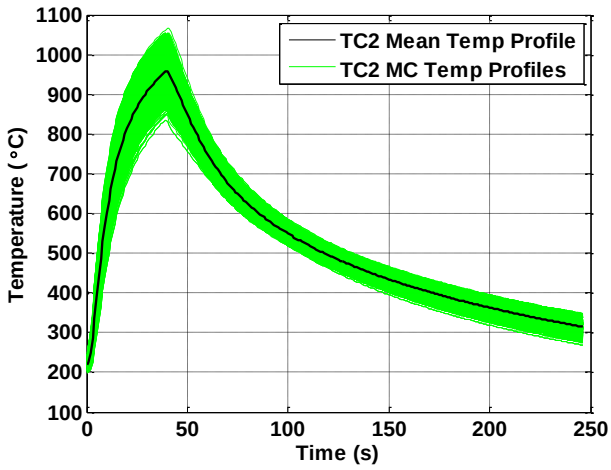

Figure 10. TC2 MC Temperature Profile Spread

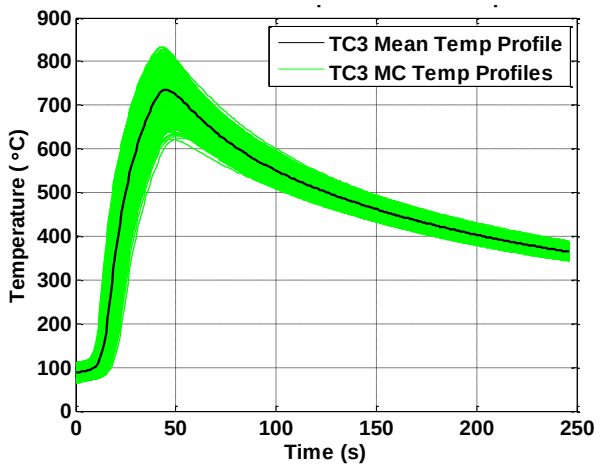

Figure 11. TC3 MC Temperature Profile Spread

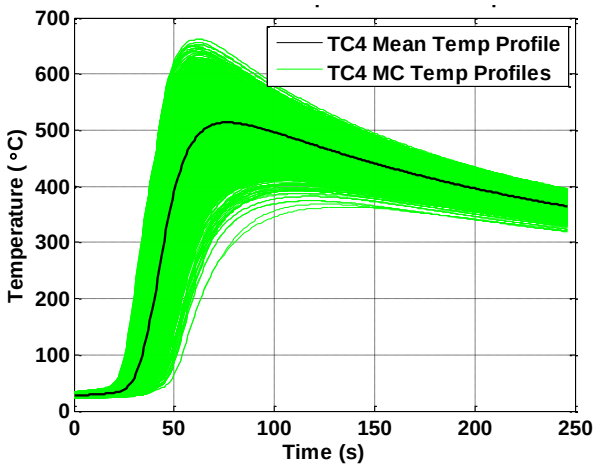

Figure 12. TC4 MC Temperature Profile Spread

After generating temperature profile predictions from approximately five-thousand randomly generated input scale factor vectors, a time-dependent linear regression analysis was performed to gain understanding of the relationship between thermal scaling parameter input uncertainties and the temperature vs. time output uncertainties at each thermocouple. The sample correlation coefficient calculation in Equation 13 below represents each parameter's contribution to prediction uncertainty. In short, this equation describes the effect of each input scale factor's contribution on each output temperature prediction profile.

$$\rho_i = \frac{\sum_{j=1}^{5000}(x_{ij}-x_{i,avg})(y_j-y_{avg})}{\sqrt{\sum_{j=1}^{5000}(x_{ij}-x_{i,avg})^2 \sum_{j=1}^{5000}(y_j-y_{avg})^2}} \tag{13}$$

The resulting analysis provided "pie charts as a function of time" showing time-dependent scaling parameter uncertainty contributions at each thermocouple location. Area charts representing scale factor contribution to overall uncertainty for TC1-TC4 is shown in Figure 13-16 below.

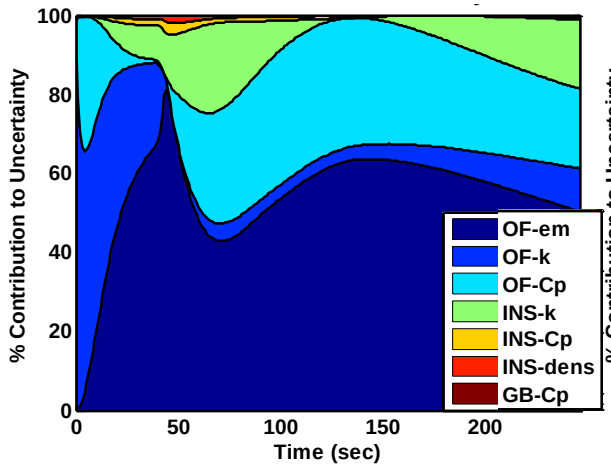

Figure 13. TC1 Contribution to Uncertainty

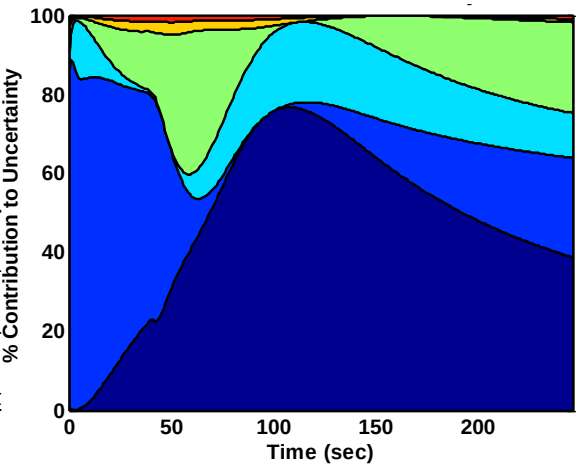

Figure 14. TC2 Contribution to Uncertainty

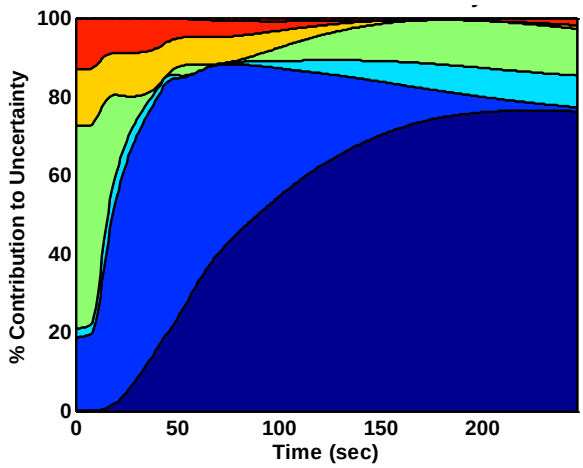

Figure 15. TC3 Contribution to Uncertainty

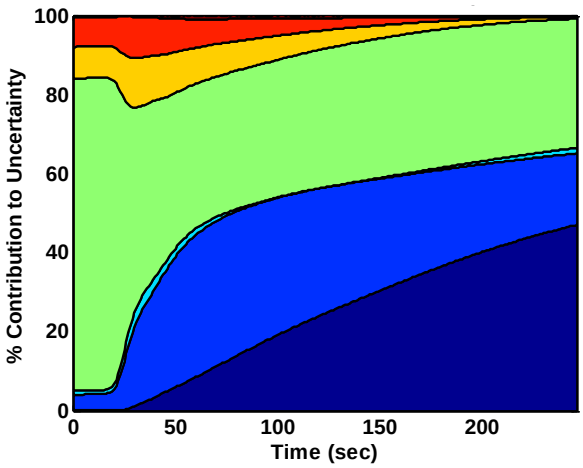

Figure 16. TC4 Contribution to Uncertainty

Some interesting comments can be made about the FTPS material properties during Run 2259 by inspecting Figure 13 – Figure 16 above. Thermal conductivity of the insulator (INS-k) is a sizeable contributor to all four thermocouples (TC1 – TC4). Its contribution to prediction uncertainty behaves very differently in the TC1 and TC2 below the top two Outer Fabric layers. In TC1 and TC2, the contribution of insulator thermal conductivity increases steadily past model retraction at t = 41s as latent heat within the top layer continues to conduct through the layup. As the cool-down process sets in and surface to ambient radiation becomes the dominant mode of heat transfer, thermal conductivity decreases significantly. As the temperature profiles slowly achieve steady state, insulator thermal conductivity becomes a large contributor once again.

In general, TC1 and TC2 are dominated by emissivity of the Outer Fabric (OF-em), thermal conductivity of the Outer Fabric (OF-k), and specific heat of the Outer Fabric (OF-Cp). The chart for TC3 also displays the same dominating material properties because the effects of one layer of insulation are still out-weighed by the effects of two layers of Outer Fabric above it. Since the LM error-minimization code uses only TC4 data in its objective function, it is most beneficial to understand Figure 16. In this chart, TC4 is clearly dominated by insulator thermal conductivity (INS-k), insulator specific heat (INS-Cp), and insulator density (INS-dens). Now, there are two layers of insulation directly above TC4 along with two layers of outer fabric. Therefore, TC4 still experiences outer fabric emissivity and thermal conductivity as significant contributors, but insulator thermal conductivity, specific heat, and density are much more significant to temperature prediction uncertainty. The remaining parameters do not contribute as significantly to prediction uncertainty, and all parameters excluding $f_{\varepsilon_{OF}}$, $f_{k_{OF}}$, and $f_{k_{INS}}$ can be set aside for LM error-minimization

Finally, a sensitivity analysis was performed for thermocouples (TC1 – TC4) of Layup 1. The primary objective of sensitivity analysis is to identify the correlation between scaling parameters and determine how much each parameter affects the absolute temperature prediction outputs. By calculating the partial derivatives of temperature outputs with respect to scaling parameter inputs and perturbing each parameter by a small amount (approximately $\varepsilon = \pm 1\%$ off nominal), one can obtain the resulting output behavior to obtain relative correlations between parameters. This calculation is similar to Equation 14 below used in the LM method algorithm.

$$X_{ij} \cong \frac{\partial T_i}{\partial P_j} = \frac{T_i(P_1, P_2, \ldots, P_j + \varepsilon P_j, \ldots, P_N) - T_i(P_1, P_2, \ldots, P_j - \varepsilon P_j, \ldots, P_N)}{2\varepsilon_0 P_j} \tag{14}$$

Due to linear-dependence, highly correlated parameters cannot be accurately estimated at the same time because it is difficult for the optimizer to distinguish their effects, which is important information to be carried over into the inverse parameter error-minimization process. The results are shown in Figure 17-Figure 20 below:

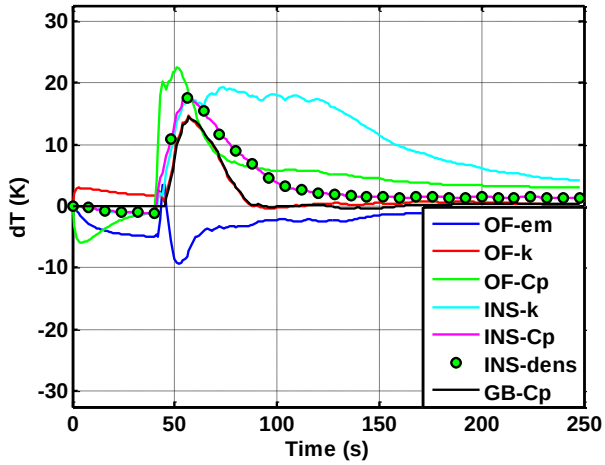

Figure 17. TC1 Scale Factor Sensitivities

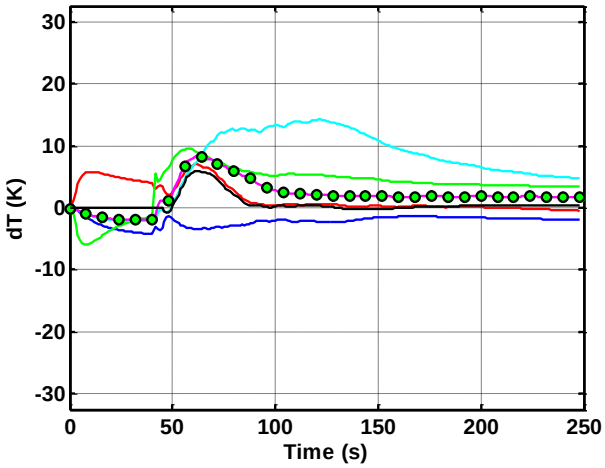

Figure 18. TC2 Scale Factor Sensitivities

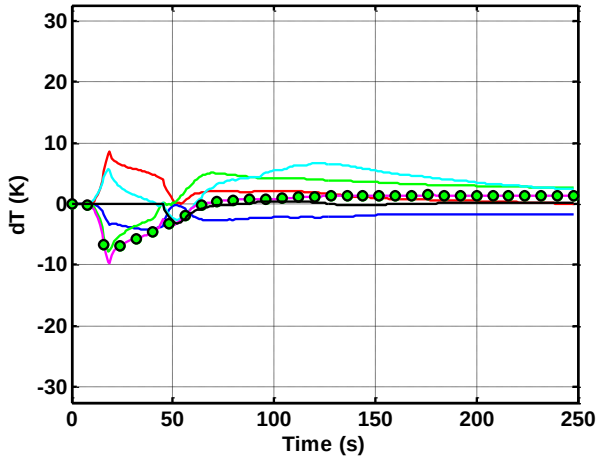

Figure 19. TC3 Scale Factor Sensitivities

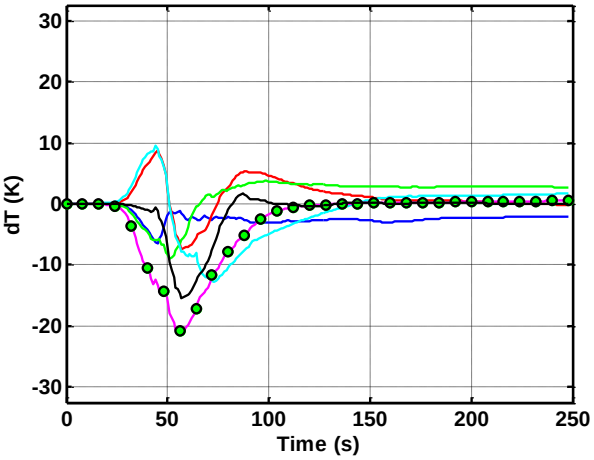

Figure 20. TC4 Scale Factor Sensitivities

The figures above display relative sensitivities of scale factors produced by an off-nominal perturbation to scale factor parameters as a function of time for each thermocouple. Some general trends for all thermocouples include 100% correlation between $f_{C_{p_{INS}}}$ and $f_{\rho_{INS}}$ along with negative correlation between $f_{\varepsilon_{OF}}$ and $f_{k_{OF}}$. Focus will be placed on Figure 20 because it shows sensitivities for TC4, which is used to calculate the LM error-minimization objective function. One can clearly see a strong positive correlation between $f_{k_{OF}}$ and $f_{k_{INS}}$, along with strong negative correlation between $(f_{k_{INS}}, f_{k_{INS}})$ and $(f_{C_{p_{INS}}}, f_{\rho_{INS}})$. Scale factor parameters that exhibit strong correlation should not be estimated simultaneously due to linear independency. Taking sensitivity analysis into consideration greatly improves convergence uniqueness and stability as a result.

The designer can now compile the information gathered in the completed uncertainty and sensitivity analyses to assist with prediction error-minimization using thermophysical scale factor parameter estimation. The information obtained from nominal, uncertainty, and sensitivity analyses for Run 2259 are as follows: focus analysis on region between heat up and TC4 bondline peak temperature, focus on estimating parameters $f_{\varepsilon_{OF}}$, $f_{k_{OF}}$, and $f_{k_{INS}}$ because they have the largest effect on prediction uncertainty, and reduce this scale factor set to $[f_{\varepsilon_{OF}}, f_{k_{INS}}]$ to avoid linear-dependency between scale factors. The results of a second parameter estimation using this reduced set of scale factors is shown in Figure 21 below:

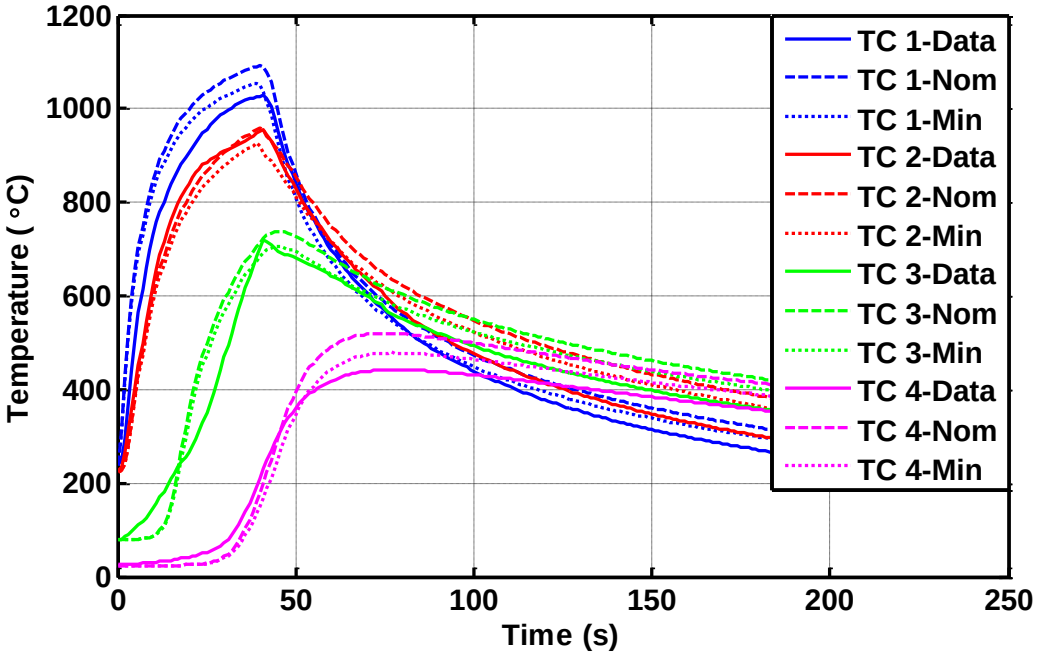

Figure 21. Error-Minimized TC-4 Bondline Predictions for Reduced Scale Factor Set

The new error-minimzed temperature prediction profile for TC4 is shown by the "TC4-Min" line in Figure 21. Compared with the initial parameter estimation shown in Figure 8, the new prediction is now significantly closer to measured arc-jet data for TC4. Despite this increased prediction accuracy and valuable reduction in the number of degrees of freedom in the thermophysical scale factor estimation vector, the thermal model predictions still suffer from significant model error.

In order to remove model error associated with the applied heat flux, a new boundary condition was enforced. The arc-jet measured TC3 temperature profile has been enforced on the thermal model to generate TC4 predictions. This is referred to as the TC driver approach using TC3 measured data to predict the TC4 temperature profile. Proving that the LM error-minimization process can result in improved thermocouple predictions for the TC driver approach is advantageous because it greatly reduces model error; it can serve as a valuable debugging tool for the LM error-minimization code and provides a simple test case to start error-minimization before addressing heat-flux uncertainties and multiple TC's in the LM error-minimization objective function.

C. Application of Parameter Estimation Methodology to TC3 Driver COMSOL Model for Run 2259

After changing the COMSOL model boundary condition to be driven by the arc-jet measured TC3 temperature profile, a similar analysis was performed in order to provide a complete, end-to-end LM error-minimization. Comparing TC4 temperature predictions with actual measurements from Run 2259 using the initial heat flux driven COMSOL model and the TC driver approach, the TC3 driver approach eliminates a great deal of model uncertainty by calculating TC4 predictions based only on heat conduction between TC3 and TC4. A verification test was performed to ensure that the error-minimizing code was performing as it should in an ideal situation. Then, a test problem is presented attempting to match TC4 predictions with Run 2259 TC4 measurements.

As a verification test, the author performed an experiment on the LM error-minimization code. The goal of this study was to compare the thermal model predictions against a known set of thermophysical parameters. To eliminate all model error, the thermal model was used to generate simulated TC4 data using only two parameters, using $f_{k_{INS}}$ and $f_{C_{p_{INS}}}$, both set at their nominal values [$f_{k_{INS}} = 1, f_{C_{p_{INS}}} = 1$]. Next, the error-minimization code was set to start with a random set of scale factors [$f_{k_{INS}} = 1.1, f_{C_{p_{INS}}} = 0.9$] and run to see if error could be minimized completely by converging on the simulated scale factor values [$f_{k_{INS}} = 1, f_{C_{p_{INS}}} = 1$].

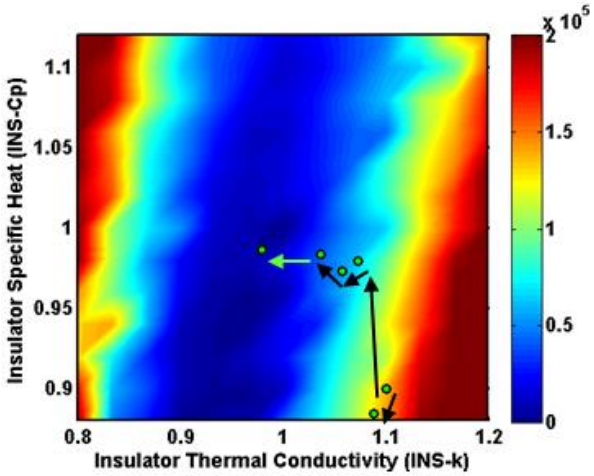

Figure 22. TC4 Simulated Data Design Space

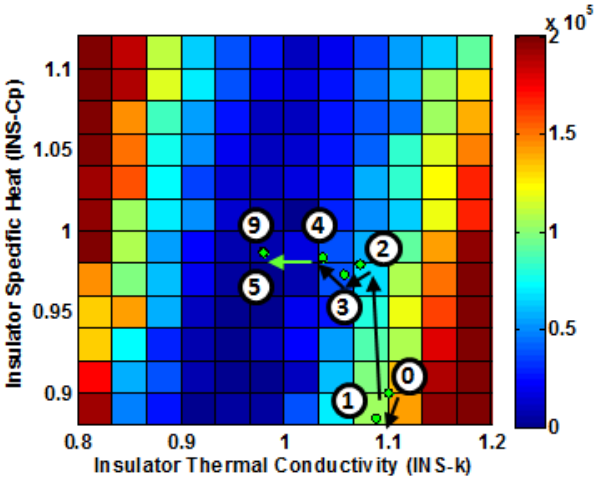

Figure 23. TC4 Simulated Data Design Space Convergence

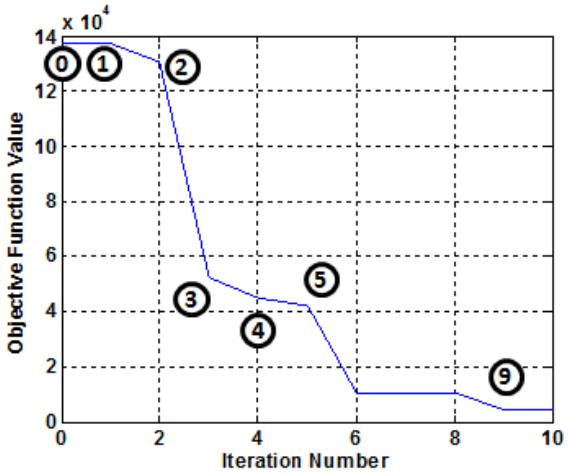

Figure 24. Objective Function Value vs. Iteration

Figure 22 – Figure 24 show the 9 iterations performed before the error-minimization code reached a steady-state solution at $[f_{k_{INS}} = 0.98, f_{C_{p_{INS}}} = 0.99]$. Although the parameter values were not recovered exactly, this is an extremely positive result showing that the LM code moves in the right direction and obtains a solution in the close neighborhood of the design space optimum. As one can see from Figure 23, the each iteration step approaches in a steepest descent fashion until it nears the minimum of the design space. Challenges with the error-minimization code occurrs when gradients become vanishingly small. Adjustments are continuously being made to Step 7 and Step 8 in the LM algorithm in order to get the code "unstuck" from pre-mature convergence and achieve a more optimal solution in later iterations. The resulting TC4 temperature profile prediction is shown in Figure 25 below, which shows very close agreement between the simulated data curve, "TC4-Data", and the error-minimized prediction curve, "TC4-Min i=9".

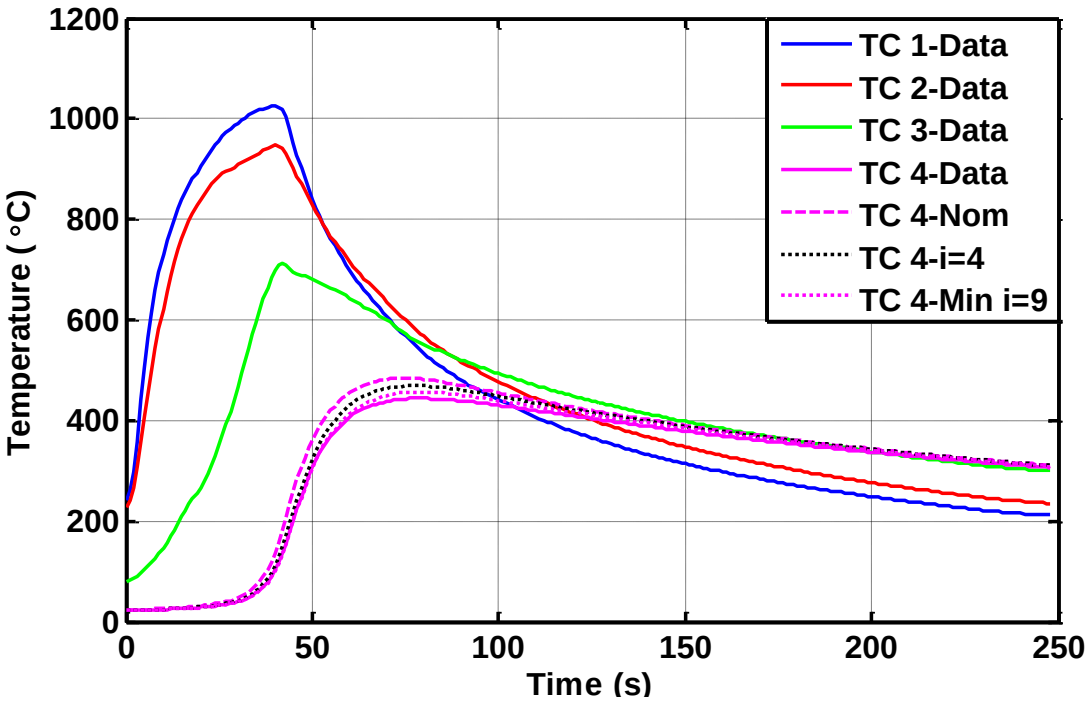

Figure 25. Error-Minimized TC-4 Bondline Predictions for TC3 Driver Simulated Data

Similar to the previous section, the nominal analysis suggests that only the region between model injection and peak TC4 bondline temperature be included in the objective function evaluation in order to remove model error from the cool-down process. In other words, the LM error-minimization objective function only considered prediction differences between t = 0 seconds and t = 78 seconds. A similar uncertainty analysis was performed for the second insulator layer in Figure 26 and Figure 27 below. Using the new TC3 driven boundary condition, heat is conducted from TC3 through the second insulator layer to predict TC4 temperatures. The uncertainty analysis below suggests that $f_{C_{p_{GB}}}$ is the scale factor that contributes the least to prediction uncertainty and can be set aside. Additionally, a sensitivity analysis was performed on TC4 using the remaining parameters. Due to strong correlation between $f_{C_{p_{INS}}}$ and $f_{\rho_{INS}}$, the $f_{\rho_{INS}}$ scale factor was set aside.

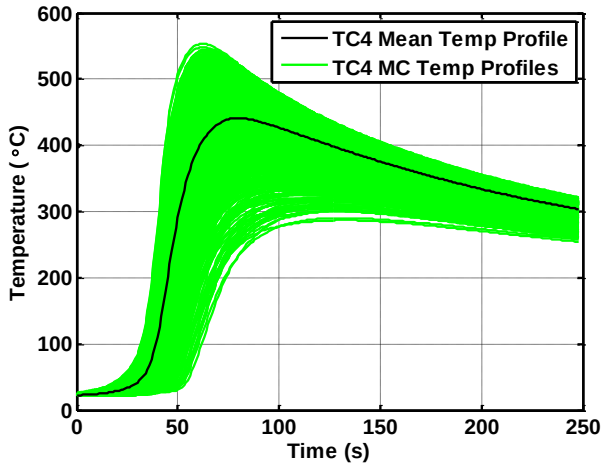

Figure 26. TC4 MC Temp. Profile Spread

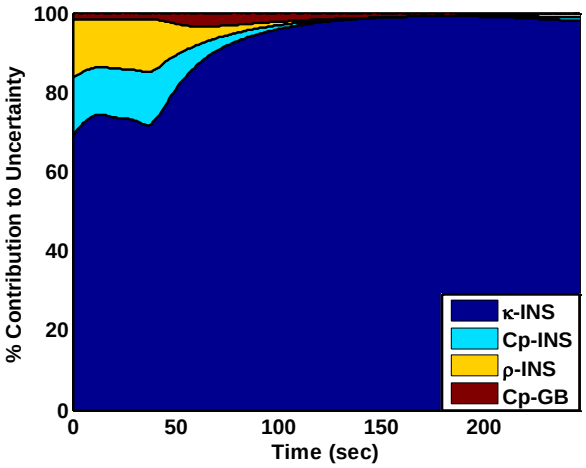

Figure 27. TC4 Contribution to Uncertainty

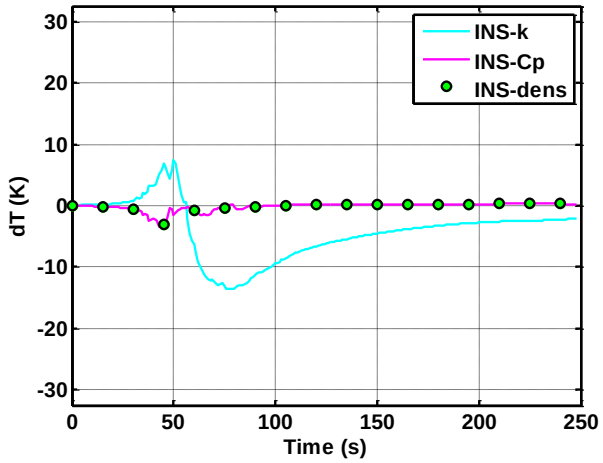

Figure 28. TC4 Scale Factor Sensitivities

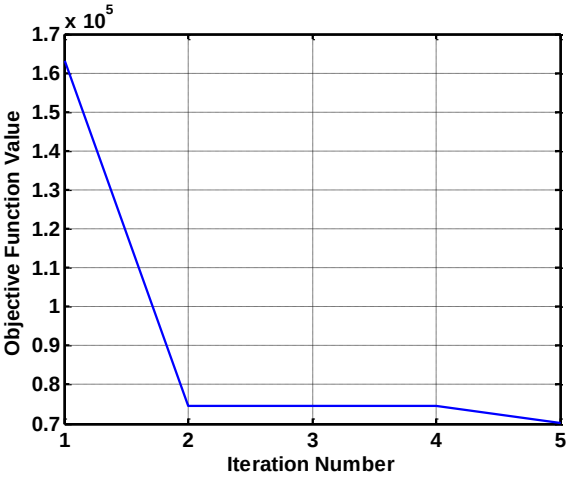

Figure 29. Objective Function Value vs. Iteration

Figures 29 – Figure 31 are the results from performing an LM error minimization using $f_{k_{INS}}$ and $f_{C_{P_{INS}}}$ between model injection at t=0 seconds and TC4 bondline peak at t = 78 seconds. Figure 30 and Figure 31 show successful LM error-minimization with iteration history provided in Figure 29.

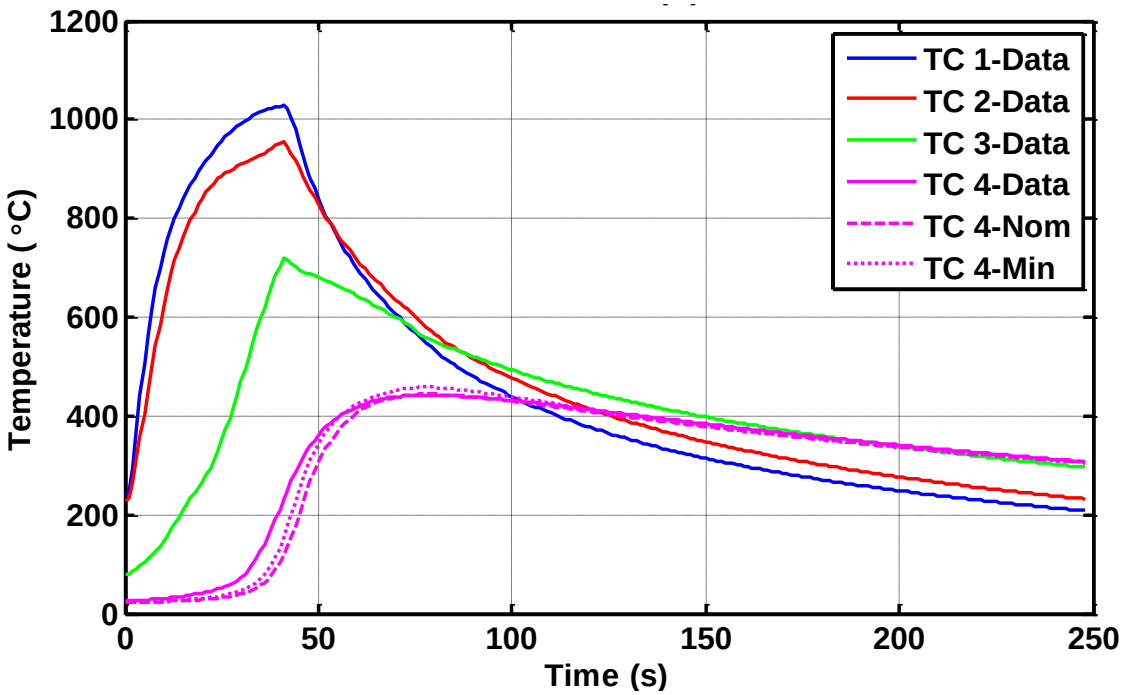

Figure 30. TC Driver Boundary Conditions Applied at TC3 – Error-Minimized TC4 Prediction

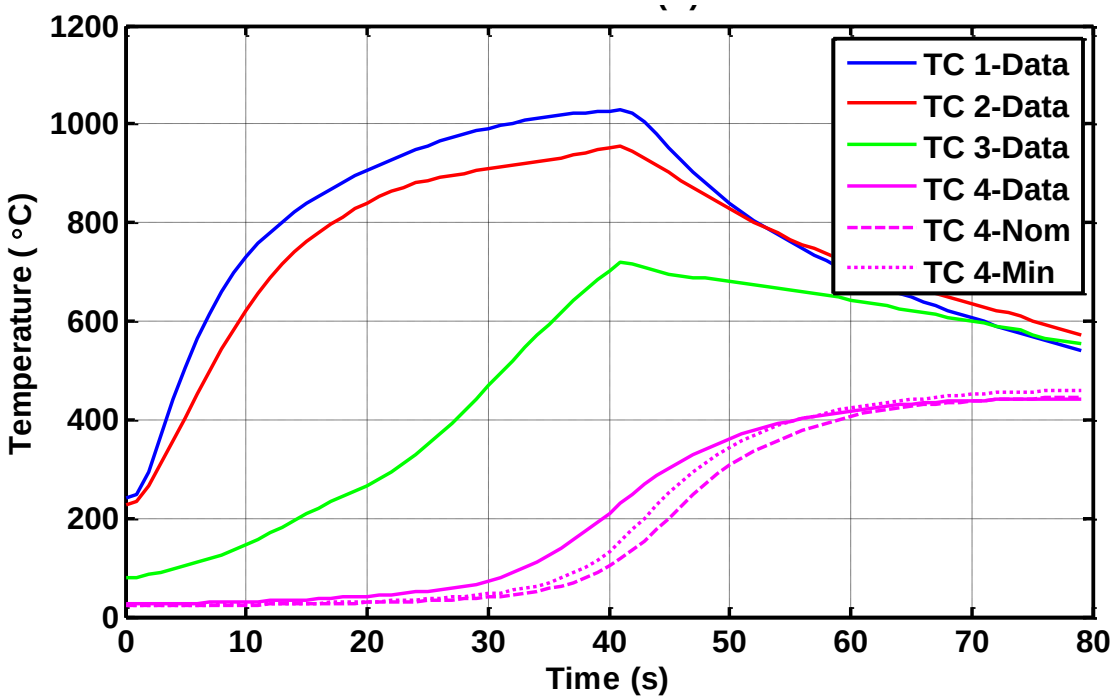

Figure 31. TC Driver Boundary Conditions Applied at TC3 – Error-Minimized TC4 Prediction

Successful LM error-minimization shown in Figure 31 is a promising result that sets the stage for broadening this method to higher fidelity physics models, multiple thermocouples, various test conditions, and various FTPS layups.

VI. Conclusions and Future Work

A Flexible Thermal Protection System (FTPS) stack was arc-jet tested in the Boeing LCAT facility to characterize thermal material performance for future HIAD applications. A physics-based thermal model was created using COMSOL in order to accurately predict measured thermocouple temperatures at multiple depths. After noticing a large modeling discrepancy with initial predictions, the LM technique was implemented for error minimization by estimating thermophysical properties embedded in the COMSOL model. Through use of an established parameter estimation methodology, valuable insight about solution uniqueness and stability was used to improve the thermophysical parameter estimation process. The boundary condition of the thermal model was changed to being driven by the thermocouple temperature profile rather than measured heat flux to reduce model discrepancy. Using this TC driver approach, the LM method was implemented over a nominally selected range to reduce prediction error of the bondline thermocouple.

Although the error-minimized prediction curves in Figure 30 and Figure 31 did not match up perfectly to test data, there are a few things that could explain the current discrepancy. Run 2259 is a shear-test run, which contains variability of pressure and heat flux on the surface of the sample. This makes it difficult to correctly estimate the correct heat flux to input into the thermal model. To address this problem, the error-minimization code will be run using the universally accepted +/- 10% arc-jet heating boundary condition. Additionally, the current heat flux driver analysis minimizes prediction discrepancies using only the bondline thermocouple. The inaccurate predictions for other thermocouples skews predictions for the bondline thermocouple (TC4). Future analysis plans to include all thermocouples in the LM error-minimization objective function in order to make all thermocouple predictions match with measured test data.

The long-term goal of this research is to develop a robust error-minimization methodology that can be applied across a wide range of candidate FTPS materials. The resulting error-minimization technique will be extended to similar layups and exposed to various arc-jet heat fluxes and pressure combinations in an effort to extend thermal model development. The current research shows a successfully implemented LM error-minimization to reduce temperature prediction discrepancies from arc-jet thermocouple measurements. This increased modeling precision results in a more efficiently margined FTPS for a HIAD and ultimately a mass savings for the entire mission.

Acknowledgments

The authors are very grateful for the help of Dr. John Dec and Steven Tobin for their invaluable assistance with analyzing Boeing LCAT FTPS test data. Also, the author would like to graciously thank Dr. Robert Braun and Dr. Milad Mahzari for direction and guidance on this research topic. Additionally, we are grateful for all those participating in the Boeing LCAT testing campaign and the IRVE-3 flight demonstration. Thank you for making this research possible.

References

[1]Edquist, K., Dyakonov, A., Wright, M., Tang, C., "Aerothermodynamic Design of the Mars Science Laboratory Heatshield," *41st AIAA Thermophysics Conference*, San Antonio, TX, June 22-25, 2009, AIAA Paper 2009-4075.

[2]Braun, R., Manning, R., "Mars Exploration Entry, Descent and Landing Challenges," in IEEEAC paper #0076, December 2005.

[3]Del Corso, J., Bruce III, W., Hughes, S., Dec, J., Rezin, M., Meador, M. A., Guo, H., Fletcher, D., Calomino, A., Cheatwood, F., "Flexible Thermal Protection System Development for Hypersonic Inflatable Aerodynamic Decelerators," *9th International Planetary Probe Workshop*, Toulouse, France, June 16-22, 2012.

[4]Hughes, S., Cheatwood, F., Dillman, R., Wright, H., Del Corso, J., "Hypersonic Inflatable Aerodynamic Decelerator (HIAD) Technology Development Overview," *21st AIAA Aerodynamic Decelerator Systems Technology Conference and Seminar*, Dublin, Ireland, May 23-26, 2011, AIAA Paper 2011-2524.

[5]Bruce III, W., Mesick, N., Ferlemann, P., Siemers III, P., Del Corso, J., Hughes, S., Tobin, S., Kardell, M., "Aerothermal Ground Testing of Flexible Thermal Protection Systems for Hypersonic Inflatable Aerodynamic Decelerators," *9th International Planetary Probe Workshop*, Toulouse, France, June 16-22, 2012.

[6]Internal work performed by John Dec and Steven Tobin, NASA Langley Research Center

[7]Tobin, S., Dec, J., Mesick, N., "Flexible Thermal Protection System Candidate Layup Configurations", NASA Langley Research Center, Hampton, VA, 2012 (unpublished).

[8]Özisik, M., Orlande, H., *Inverse Heat Transfer: Fundamentals and Applications*, Taylor and Francis, New York, 2000.

[9]Mahzari, M., "An Inverse Parameter Estimation Methodology for the Analysis of Aeroheating and Thermal Protection System Experimental Data," *42nd AIAA Thermophysics Conference*, Honolulu, Hawaii, June 27-30, 2011, AIAA Paper 2011-4027.

[10]Vanderplaats, G., *Multidiscipline Design Optimization*, 1st ed., Vanderplaats Research & Development, Inc., Colorado Springs, CO, 2007, pp. 103-109.

[11]Molavi, H., Hakkaki-Fard, A., Pourshaban, I., Mahbubi Fard, M., and Rahmani, R. K., *Estimation of Temperature-Dependent Thermophysical Properties of Noncharring Ablator*, Journal of Thermophysics and Heat Transfer, Vol. 23, No. 1, 2009. pp. 50-58.

[12]Beck, J.V., "Transient Determination of Thermal Properties," *Nuclear Engineering and Design*, Vol. 3, No. 3, 1966, pp. 373–381.